Investigation of the tin-doped phosphor (Sr,Mg)$_3$(PO$_4$)$_2$:Sn^{2+} for fluid temperature measurements

Benoît Fond,[*] **Christopher Abram, Miriam Pougin and Frank Beyrau**

Lehrstuhl für Technische Thermodynamik, Otto-von-Guericke-Universität Magdeburg, Magdeburg, Germany
[*]*benoitfond@gmail.com*

Abstract: The photoluminescence properties of the phosphor (Sr,Mg)$_3$(PO$_4$)$_2$:Sn^{2+} were investigated for luminescence thermometry in fluids. The luminescence emission intensity at 300 K is on the order of 10^6 photons per particle and the lifetime is 26 μs. With increasing temperature, the wide emission band exhibits a pronounced blue shift which can be exploited for temperature imaging using a two-colour ratiometric approach. The measured temperature sensitivity in an imaging configuration is 0.6%/K at 300 K. The T$_{50}$ quenching temperature is 650 K, similar to the phosphor BaMgAl$_{10}$O$_{17}$:Eu^{2+}, but the estimated temperature sensitivity at 700 K is a factor 7 higher (0.36%/K). Moreover, the excitation laser fluence has a negligible effect on the measured temperature (0.6 K for a 10% change in the fluence), a five-to-tenfold improvement over phosphors previously investigated for fluid thermometry. The phosphor (Sr,Mg)$_3$(PO$_4$)$_2$:Sn^{2+} therefore offers significant improvements for thermometry applications in turbulent flows in the 300-900 K range.

1. Introduction

Fluid temperature measurements are key to furthering our understanding of a variety of phenomena involving heat transfer, buoyancy, phase changes or chemical reactions found in systems ranging from industrial energy devices such as gas turbines to natural processes, such as thermal convection. Over the past 10 years, thermographic phosphor particles, which are temperature-sensitive luminescent materials, have experienced a rise in use as tracers for point and 2-D measurements in fluids (see review article [1]). Most phosphors do not participate in chemical reactions, many host compounds (e.g. oxides) have a high melting point, the luminescence properties are often insensitive to the gas composition and pressure, and they can be used in both liquid and gas flows, making phosphor particles very suitable as a tracer material. The same particles can also be used for simultaneous velocity measurements using particle-based velocimetry approaches to obtain combined temperature-velocity measurements, such as the Thermographic Laser Doppler Velocimetry or [2] or Thermographic Particle Image Velocimetry [3] approaches. Phosphors have been used in many applications, with examples including liquid film absorbers [4], internal combustion engines [5] and gas turbine film cooling flows [6].

For a particular application the choice of phosphor particles plays a central role in the precision and accuracy of the optical thermometer. The critical luminescence properties are: a) the luminescence emission intensity for the conditions of the experiment, e.g. particle number density in the fluid, excitation fluence and temperature range; b) the luminescence lifetime, which imposes a limit on the minimum measurement duration; and c) depending on the thermometry approach, the sensitivity of the luminescence emission lifetime or emission spectrum to temperature. Fortunately a huge variety of potential compounds exists and among these the

luminescence lifetime and temperature sensitivity of more than hundred materials are known [7]. That said, only a dozen phosphors have been used in the context of fluid thermometry [1]. Those covered a wide range of lifetimes and temperature sensitivities. Recently, the emission of six of those phosphors were compared using dispersed particle methods, finding that the luminescence emission intensity of ZnO, $BaMgAl_{10}O_{17}$(BAM):Eu^{2+} and Mg_4FGeO_4(MFG):Mn^{4+} were similar and on the order of 10^6 photons per particle at an excitation fluence of a 20 mJ/cm^2 [8]. For $Y_3Al_5O_{12}$(YAG):Pr^{3+}, YAG:Dy^{3+} and La_2O_2S:Eu^{3+}, the emission intensities of the emission bands used for thermometry were found to be several orders of magnitude lower than this, even for significantly higher laser fluences. The luminescence lifetimes of ZnO and BAM:Eu^{2+} is 1 μs or shorter, very suitable for measurements in fast turbulent flows, while that of MFG:Mn^{4+} is on the order of a few ms which rules out its use in all but very slow fluid flows.

ZnO is rapidly quenched with increasing temperature, with a T_{50}, the temperature at which the emission intensity is 50% of its room temperature value, of 400 K. BAM:Eu^{2+} can be used for thermometry at higher temperatures with a T_{50} of 700 K. For both phosphors, the shift and broadening of their emission bands with temperature can be exploited for temperature imaging using a two-colour intensity ratio approach. At seeding densities of 2×10^{11} particles/m^3, a temperature precision of 3 and 10 K could be achieved around room temperature for ZnO and BAM:Eu^{2+} respectively [9]. The higher precision achieved with ZnO is afforded by the more pronounced shift of the emission band with temperature. However, ZnO particles exhibit an unfortunate and strong cross sensitivity to the excitation fluence, amounting to a 6 K error per 10% change in the laser fluence. This can often be corrected for, and a discussion of laser fluence corrections and the effect of the fluence cross-dependency on the measurement accuracy can be found in Refs. [1, 9]. However, ZnO definitely cannot be used in situations where unsteady refractive index inhomogeneities are present, which causes so-called striping in the measured temperature field.

There is a clear motivation to find alternative phosphors with 1) a similar or even higher signal level and a delayed onset of thermal quenching; 2) a higher temperature sensitivity; 3) a negligible cross-sensitivity to the laser fluence. This article describes the investigation of another phosphor material, strontium magnesium orthophosphate doped with divalent tin: $(Sr,Mg)_3(PO_4)_2$:Sn^{2+}. While to our knowledge, tin-activated phosphors have not been exploited for thermometry before, $(Sr,Mg)_3(PO_4)_2$:Sn^{2+} has been a prominent phosphor material used in the lighting industry and so first some available literature data is reviewed to rationalise our selection.

$(Sr,Mg)_3(PO_4)_2$:Sn^{2+} was extensively used in the 1960's as the red component in fluorescent and high-pressure mercury vapour lamps, since it is efficiently excited by both low and high pressure mercury vapour emissions. Though it was later substituted in fluorescent lamps by the narrow-band YVO_4:Eu^{3+}, which presents better colour characteristics, $(Sr,Mg)_3(PO_4)_2$:Sn^{2+} is still in use today in high colour rendering lamps due to its broad emission band. The location and width of the emission band observed in Sn^{2+}-activated compounds is strongly dependent on the host crystal phase [10]. $(Sr,Mg)_3(PO_4)_2$:Sn^{2+} has a broad emission band centered in the red region (600-650 nm) at room temperature, which is only observed in $Sr_3(PO_4)_2$ systems when Sr is partially replaced by either Mg, Ca, Zn, Al or Cd to form a crystal phase similar to that of β-Ca_3PO_4 [11]. The solid solution with a substitution of 11 mol % of Mg and a dopant concentration (Sn to 2P ratio) of 2 mol % was considered optimal in terms of quantum efficiency and temperature stability by Sarver et al. [12]. The red emission band has a quantum efficiency in the 90-100% range of that of the reference phosphor $MgWO_4$ [12], which itself is reported to have an efficiency of 85% [13]. The luminescence transitions involved in the emission are very different from those found in the two phosphors mentioned above. In ZnO, interband transitions are responsible for the exploited emission band and in BAM:Eu 4f5d → 4f transitions of the Eu^{2+} ion are used. In $(Sr,Mg)_3(PO_4)_2$:Sn^{2+}, the Sn^{2+} ion has a $5s^2$ electronic configuration, and the transition responsible for the red emission band is of the 5s5p → $5s^2$ type. Decay times in the

order of several microseconds have been reported in tin-doped coumpounds [14, 15], which would be suitable for fluid thermometry. The excitation spectrum is a broad band with a maximum at 260 nm, with the intensity decreasing to 5% at 355 nm (the third Nd:YAG harmonic which is convenient for excitation) [16].

Some information is known about the spectral changes of the luminescence emission with temperature because this colour change is seen as detrimental to performance in colour-rendering lamps [16]. The main emission band shifts and widens towards the blue spectral region with increasing temperature. A small emission band representing 5% of the energy is also present at 400 nm at room temperature [12]. The phosphor exhibits relatively favourable thermal quenching characteristics. The T_{50} temperature, the temperature at which the emission intensity has decreased by 50% with respect to the room temperature value, appears to be between 600 and 700 K depending on the activator concentration [16]. Thermal stability was also studied. Exposures of the phosphor in air for 30 mins at 630°C, and 730°C, led to a reduction in room temperature brightness of 10% and 57%, respectively [12]. The thermal stability is similar in terms of the temperature/heat treatment duration space to that of BAM:Eu^{2+} [17, 18]. Note that this is not a concern for short residence times of the particles at high temperatures when used in flows. BAM:Eu^{2+} was found to have unchanged luminescence properties after exposure to the high-temperature reaction zones of a non-premixed hydrogen flame (0.1 s above 1700 K) [19].

The high quantum efficiency, the prounounced shift of the emission spectrum with temperature and the favourable thermal quenching characteristics reported for this material together with the short lifetime of the $5s5p \rightarrow 5s^2$ emission in Sn^{2+}-doped compounds form an attractive combination of properties as a thermometry sensor. In this paper, the luminescence properties of micron-size $(Sr,Mg)_3(PO_4)_2$:Sn^{2+} particles (referred to in the following as SMP:Sn^{2+}) are investigated for use as temperature sensors in fluids. The luminescence lifetime is measured, and using liquid suspensions and particle counting, the emission intensity per particle is quantified using pulsed laser excitation. The temperature sensitivity is evaluated in an imaging configuration. Cross-sensitivities to excitation fluence and particle number density are also probed. Emission spectra are recorded over the 300-900 K to assess the useful temperature sensing range. The overall thermometric performance of this phosphor is finally compared to that of ZnO and BAM:Eu^{2+}.

2. Experimental methods

2.1. Material characterisation

A commercial SMP:Sn^{2+} powder supplied by OSRAM (SV 253) was investigated in this study. The median volume equivalent sphere diameter was about 10 μm as specified by the manufacturer. The density of the phosphor is 3.9 g/cm^3. This powder size is unsuitable for flow tracing as it has response times on the order of several milliseconds in air [3]. The powder was ground and de-agglomerated to obtain a finer grade. The resulting size distribution was determined by a Coulter counter (Beckman Multisizer 3), with 300 size steps of 100 nm, starting from 1μm. The particles were imaged using a scanning electron microscope (SEM) and the composition was evaluated using an energy-dispersive X-ray spectroscopy system coupled into the SEM.

The heat capacity is an important quantity for applications of phosphor particles for thermometry in fluids, as the response time of a particle to fluid temperature changes scales linearly with the heat capacity [1]. Differential scanning calorimetry of the powder was performed. A small sample of the powder (26 mg) was heated at a rate of 20 K/min from 300 K to 1400 K. Al$_2$O$_3$ was used as a reference sample. The heating was repeated three times. To study the thermal stability, a larger sample of the powder was heated in a tube furnace at the same rate up to 900 K, and its luminescence properties (emission intensity and spectrum) at room temperature were analysed and compared to those of the untreated sample.
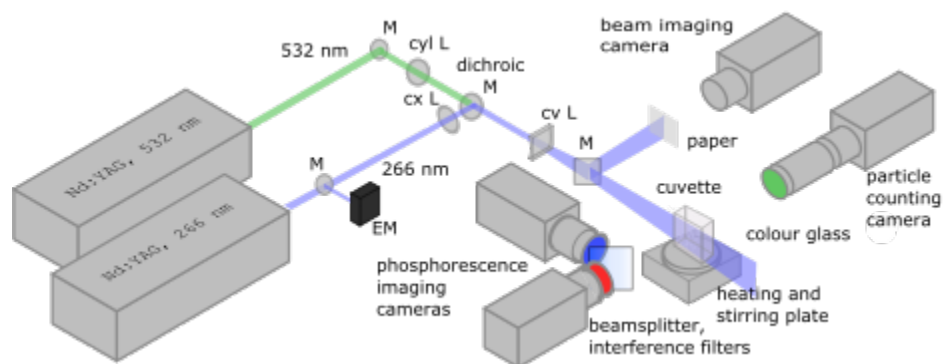
Fig. 1: Setup for two colour imaging system including particle counting and 2-colour intensity ratio imaging system. The abbreviations used in the sketch are: EM-energy monitor, L-lens, M-mirror, cv-concave, cx-convex, cyl-cylindrical. Note that counting and two colour detection were not performed simultaneously

2.2.   Liquid dispersion and particle counting

To determine the emission intensity of phosphor particles on a per particle basis as well as to determine cross-sensitivity to parameters such as the laser fluence or the seeding density, phosphor particles must be characterised in the dispersed form. This is for two reasons. The first is to avoid effects which are far more pronounced in the bulk powder form than in the dispersed form, such as heating and degradation of the powder under repeated illumination, amplified spontaneous emission, re-absorption of luminescence emission, and multiple scattering, as discussed in Refs. [20] and [1]. The second reason is that a comparison of luminescence emission intensities from powder samples may not bear any relation to the relative emission intensities measured from dispersed particles [8], which are the data relevant to fluid thermometry.

Therefore phosphor-liquid dispersions were prepared according to the method outlined in Ref. [21]. A set mass of particles were dispersed in deionised water using an ultrasonic homogeniser and dilution was used to obtain mass loads in the range of 1 to 20 mg/L. The solution was contained in a 28 mL fused silica cuvette containing a stirring bar which was placed on a magnetic stirrer and heater plate. During the measurements, the solution was stirred continuously. The temperature of the solution was monitored by a 500 μm diameter type K thermocouple.

Due to possible particle-wall attraction it is necessary to probe the quantity of dispersed particles independently of the mass load. As shown in Fig. 1, a particle counting system [20] consisting of a 170 μm-thick light sheet propagating through the cuvette and a camera equipped with a f=200 mm Nikon lens was used to acquire high-resolution Mie scattering images, from which the number density of particles in the probe volume can be determined. Further details of the setup are given in Ref. [8].

2.3.   Spectroscopy

The luminescence decay curve of SMP:Sn^{2+} bulk powder was measured using the unfocused beam of a frequency quadrupled pulsed Nd:YAG laser (266 nm) with a pulse duration of 10 ns, and detected by a non-amplified photodiode (Thorlabs DET-10 A), equipped with a spherical convex lens. A long pass colour glass filter (WG295) was placed in front of the detector to reject laser light at 266 nm. The luminescence lifetime was also probed from liquid dispersion, using a photomultiplier tube for comparison (Hamamatsu R955HA).

In order to determine the emission intensity per particle, emission spectra of liquid-particle suspensions were acquired using an imaging spectrometer (Acton Research SP300i, f=500 mm,

300 grooves/mm) combined with an interline CCD camera (Imager Pro-X 1200x1600 pixels, 7.4 μm pixel size). Unless otherwise mentioned, the width of the entrance slit was 350 μm corresponding to approximately 3.5 nm in spectral resolution. For excitation of the particles in suspension, a 2.1 mm wide and 4.3 mm high laser beam was formed in the center of the cuvette from the output of the Nd:YAG laser at either 266 or 355 nm using a single cylindrical convex lens (f=50 mm). Based on the dimensions of the probe volume, the seeding density, and the calibration of the detection system throughput, the spectrally resolved emission intensity (photons/particle/pulse/nm) was determined [8].

To measure intensity on a per particle basis, the following steps were followed: 1) a suspension was prepared for a set mass load; 2) the seeding density in the suspensions was measured; 3) the luminescence emission of the particles was probed; 4) the seeding density was recounted. It was found that the seeding density varied by less than 5% between steps 2 and 4. Therefore it was not necessary to count particles and probe the luminescence simultaneously, which simplifies the experimental setup and avoids potential cross-talk.

To evaluate the phosphor thermometric performance over a larger temperature range, a powder sample was placed in the tube furnace and excited by an unfocused laser beam at a fluence of 1 mJ/cm^2. Luminescence emission spectra were recorded between 300 K and 900 K in 100 K steps. The slit width was 100 μm corresponding to a spectral resolution of 1 nm. The spectral resolution was verified from the width of the emission lines of a low pressure mercury lamp. To evaluate thermal quenching, the spectral intensity was integrated at each temperature over the whole emission band. Previous comparisons between the thermal quenching curve obtained from particles dispersed in heated jet and from powder samples in optically accessible furnace showed good agreement [1], so furnace measurements were prefered here for experimental simplicity. Decay time measurements were also performed over this temperature range, using the non-amplified photodiode.

2.4. Two-colour imaging system

In order to demonstrate the suitability of SMP:Sn^{2+} for temperature imaging in fluids the liquid suspensions were also probed using a two colour detection system. The cuvette was illuminated with a laser light sheet at 266 nm (7×1 mm) as shown in Fig. 1. Two cameras (Imager sCMOS, 2560x2160 pixels, 6.5 μm pixel size) equipped with f = 50 mm Nikon lenses at an f-stop of 1.4 were placed at 90° from one another and a spectrally flat beam-splitter was used to form images of the same particles on both sensors. To exploit the temperature dependence of the emission spectrum in two dimensions, a bandpass filter with a central wavelength of 510 nm and a bandwidth of 84 nm (Edmund Optics 84113) was mounted on one camera, and a 645 nm long-pass coloured glass filter (Schott RG645) on the other.

3. Results

3.1. Particle size, morphology and composition

Particle sizes of the processed powder are summarised in Table 1. Note that only particles which have a sphere equivalent volume diameter larger than a micron could be sampled, which result in a bias towards larger sizes. Both the distribution by number and by volume are given. The size is suitable for flow tracing, with a 95% response time of a 2 μm spherical particle equal to 70 μs in air at room temperature.

The mass load of particles and the particle number density were related by counting suspensions prepared with two different mass loads, which were 0.9 μg/mL, and 18 μg/mL. The ratio between measured mass load and measured number density was found to be constant to within 10%, corresponding to 1.9 ±0.1 ×10^5 particles/μg. This is in good agreement with the distribution measured using the Coulter counter distribution (1.0 × 10^5 particles/μg). The difference can be
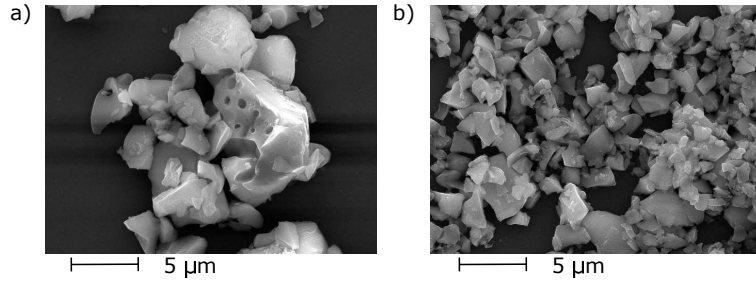
Fig. 2: Scanning electron microscope of the powder before and after grinding

attributed to the fact that particles smaller than 1 μm are counted by the particle counting system but not by the Coulter counter, resulting in a larger particle counts in the optical method.

The shape of a particle is also important for its tracing ability. For the same equivalent sphere volume diameter, non-spherical particles have a faster characteristic response time for both temperature and velocity tracing, due to their larger area to volume ratio. For further discussion, see Ref. [1] (Section 5.2). Scanning electron microscope images of the powder before and after grinding are shown in Fig. 2. The grinding and deagglomeration process has broken the large particles into many small particles with sharp edges. A large number of submicron particles can also be seen in the ground powder. The particles are non-spherical, of a shape similar to that of 2 μm BAM Eu [22], which were also obtained from grinding larger particles.

A Sn to P atomic ratio of 2% was determined from EDX, which correspond to x=0.04 in the formula $(Sr,Mg)_3(PO_4)_2:Sn_x^{2+}$ used in [16]. The Mg to Sr atomic fraction ratio was found to be 9.1%.

Table 1: Size distribution parameters of the powder after grinding and de-agglomeration

	d_{mean} (μm)	d_{median} (μm)	d_{10} (μm)	d_{90}(μm)
By volume	2.62	1.94	1.25	3.34
By number	1.52	1.40	1.06	2.12

3.2. Heat capacity and thermal stability

The results of the DSC measurements are shown in Fig. 3. During the first heating run features in the trace were observed from 400 and 500 K, and from 700 to 900 K. These features were not observed in subsequent heating runs. These might be linked with the evaporation of the powder moisture and/or exothermic reactions of residual fluxes from the synthesis process, especially after the grinding operation. To study whether the luminescence properties were altered during the first heating cycle, the emission spectrum of a sample that underwent the same heat treatment in a tube furnace was compared to that of an untreated sample. No differences in the shape of the emission spectrum could be observed, and the emission intensity was within the repeatability of the measurements (20%). It can be concluded that the changes observed in the DSC for the first heating have a negligible influence on the luminescence properties of the phosphor.

The heat capacity was extracted from the second heating curve. It is seen to increase linearly from 800 to 1600 J/kg/K in the range 400 to 1400 K. Extrapolation to room temperature yields a value of 700 J/kg/K. The volumetric heat capacity of this phosphor, SMP:Sn^{2+} is 3.1 J/K/cm^3, similar to that used in the heat transfer analysis of Ref. [3] (2.8 J/K/cm^3).
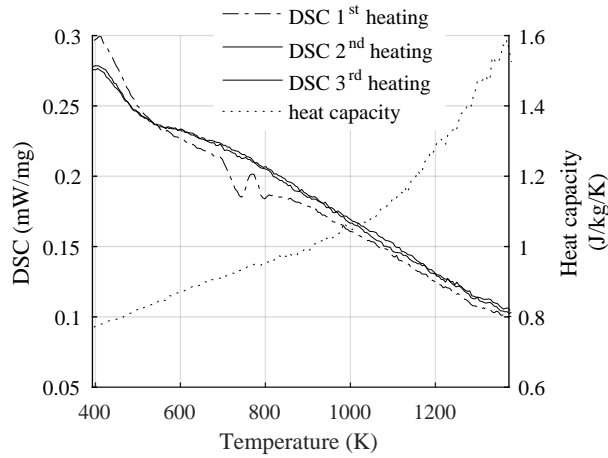
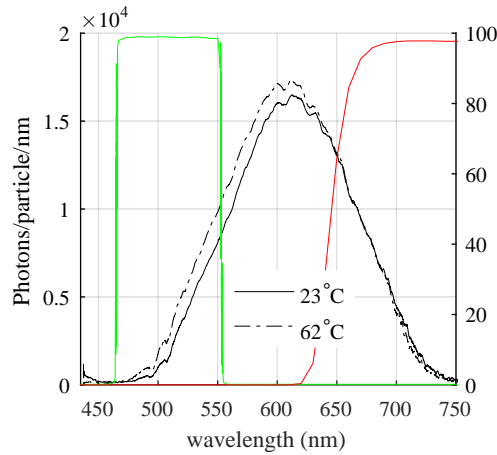Fig. 3: Differential scanning calorimetry of $(Sr,Mg)_3(PO_4)_2:Sn^{2+}$ powder and measured heat capacity

Fig. 4: Spectrally-resolved number of photons emitted per particle of 2 μm $(Sr,Mg)_3(PO_4)_2:Sn^{2+}$ particles following each laser pulse at a fluence of 20 mJ/cm^2 at 266 nm at fluid temperatures of 23 and 62°C. The filter curves used in section 2.4 are also shown
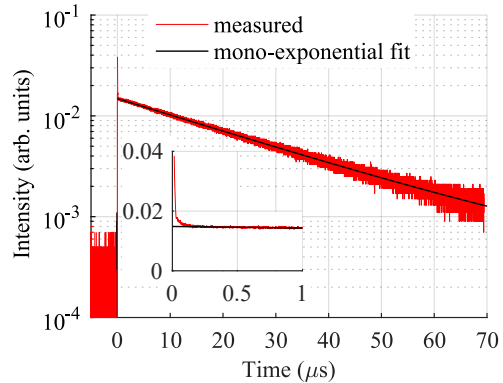

Fig. 5: Luminescence decay curve of $(Sr,Mg)_3(PO_4)_2:Sn^{2+}$ bulk powder including mono-exponential fit. The inset curve is a linear plot corresponding to early times (t<1μs)

3.3. Room temperature luminescence lifetime and emission spectrum

Emission spectra obtained from dispersed particles at 23 and 62°C are shown on Fig. 4. At 300 K the emission consists of a wide band centered at 614 nm with a full width at half maximum of approximately 125 nm.

The recorded decay curve following pulsed excitation is shown in Fig. 5. The mono-exponential decay fitted using a Levenberg Marquardt algorithm to the data between 5 and 50 μs after the laser pulse is also shown. The 1/e lifetime is 26.3 μs. As shown in the inset curve for early times (t < 1μs), there may be some faster signals with a lifetime of <100 ns, but those have a negligible
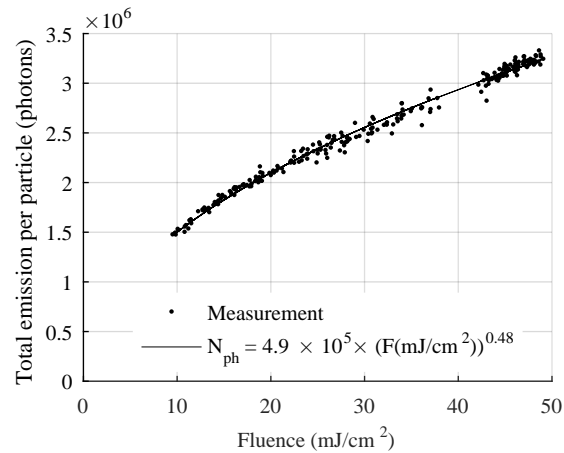
Fig. 6: Emission intensity per particle as function of the excitation fluence

impact in terms of cumulated time-integrated intensity. The lifetime measured with a PMT in the liquid suspensions was found to be in the range of 24-27 μs, matching the lifetime in the powder state, which rules out quenching of the luminescence by energy transfer with the solvent (here, water), as this can be the case for nanoparticles [23].

3.4. Emission intensity per particle

By integrating over the whole quantitative spectrum in Fig. 4, the total number of photons emitted per particle is 2.3×10^6 photons using 266 nm excitation at a fluence of 20 mJ/cm^2.

The dependence of the emission intensity per particle on the excitation fluence is important to predict the detected signal level in different experimental configurations, as well as to estimate the effect of non-linearity on the broadening of the laser sheet thickness (see Ref. [1]). The dependence of the emission intensity of the SMP:Sn^{2+} particles on the fluence between 10 and 50 mJ/cm^2 is displayed on Fig. 6. A power law fit is used to examine the departure from a linear behaviour. In the investigated range, the dependence on the laser fluence is sublinear, with a 0.48 exponent. Sublinear dependence were also observed for ZnO [9], and BAM:Eu^{2+} [20, 22, 24].

The emission intensity per particle under 355 nm excitation was also examined. Due to the weaker signal, a higher excitation fluence of 430 mJ/cm^2 was necessary. The emission intensity per particle at this fluence was found to be 7.4×10^4 photons, a fraction (3.5%) of the emission intensity for 266 nm excitation using a fluence 20 times higher. In conclusion, using a frequency tripled Nd:YAG laser for excitation does not seem to be a viable option for fluid thermometry experiments. Interestingly, the difference in emission intensity between 355 nm and 266 nm excitation is far more pronounced in these measurements on dispersed particles than what the photoluminescence excitation spectrum, which is typically obtained from thick powder samples, indicates. This may be attributed to differences in optical thicknesses between the two states, which are discussed in [8].

3.5. Temperature dependence in liquid dispersions

The emission spectra recorded at 23°C and 62°C are displayed in Fig. 4. As shown, the spectrum shifts to the lower wavelength range and broadens with increasing temperature, which is in agreement with the observation of Yen et al. [16]. The same behaviour was also observed for YPO$_4$:Sb^{3+}, and Sb^{3+} and Sn^{2+} share the same electronic structure (5s^2) [25]. The broadening of the emission band with temperature is a phenomenon which is well described by quantum

mechanical oscillators and which can be quantified by the Hyang-Rhys parameter [26]. The reasons for the shift of the emission peak toward higher energies are not entirely clear to the authors and potential explanations involve higher order coupling of the ion-lattice interaction model [26] or the thermal distribution within the emitting state $^3P_1$, which is split due to the Jahn-Teller interaction [10, 27].

Using the two camera system intensity ratio images were obtained at different liquid temperatures between 25 and 65°C at an excitation fluence of 20 mJ/cm^2. Spatially averaged intensity ratios are plotted in Fig. 7. From these results, the temperature was fitted as a second-order polynomial function of the intensity ratio (i.e. $T = a_1\varphi^2 + a_2\varphi + a_3$ where T and φ are the temperature and intensity ratio, respectively). By inverting the polynomial, the temperature sensitivity expressed as $\frac{1}{\varphi}\frac{d\varphi}{dT}$ was calculated, and plotted on Fig. 7. The resulting ratio sensitivity is approximately 0.6%/K over this range.
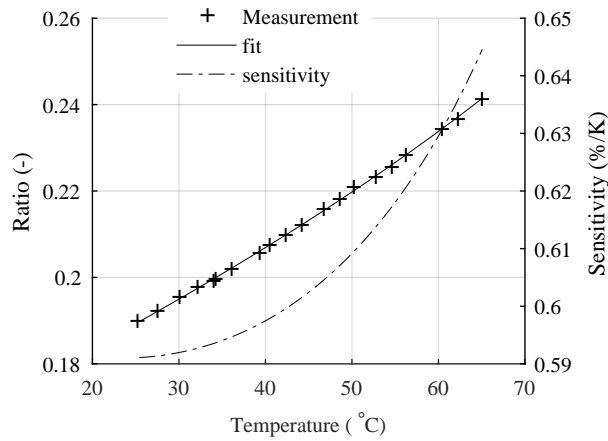

Fig. 7: Temperature dependence of the intensitiy ratio from suspended $(Sr,Mg)_3(PO_4)_2$:Sn^{2+} and derived temperature sensitivity

3.6. Effect of the excitation fluence on the intensity ratio

Intensity ratio images were acquired from suspensions of SMP:Sn^{2+} at room temperature under varying excitation fluence, and converted to temperature based on the calibration curve of Fig. 7 performed at 15 mJ/cm^2. The difference between the temperature indicated by the phosphor and that indicated by the thermocouple is plotted in Fig. 8 for fluences varying between 10 and 50 mJ/cm^2. An increase in the excitation fluence leads to an increase in the indicated temperature. The same effect was observed with ZnO and BAM:Eu^{2+}, and can be attributed to a possible combination of non-linear optical effects and laser-induced heating. The magnitude of this cross sensitivity can be derived from the exponential fit as $\frac{1}{F}\frac{dT}{dF}$, where F and T are the laser fluence and indicated temperature, respectively. If the laser varies by 10% around 20 mJ/cm^2, the indicated temperature varies by less than 0.6 K for SMP:Sn^{2+}.

3.7. Effect of the seeding density on the intensity ratio

For phosphors where the excitation and emission spectra overlap, part of the luminescence light emitted by the phosphor particle can be re-absorbed by other particles on the optical path. This can cause the indicated temperature to depend on the number of particles on the beam path, therefore on the seeding density. This is not the case for SMP:Sn^{2+} since excitation and emission spectra are well separated. However, the broad emission band may not equally scattered by

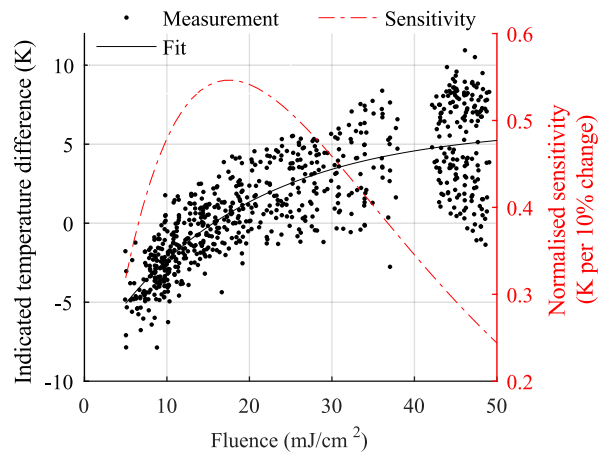Fig. 8: Indicated temperature difference as a function of excitation fluence for $(Sr,Mg)_3(PO_4)_2{:}Sn^{2+}$ at 300 K, including exponential fit, and sensitivity derived from the fit

particles on the beam path due to the dependence of particle Mie scattering on the wavelength of the light, which can also cause a dependence on the number of particles on the optical path. To investigate this possibility, a 27 μg/mL concentration solution (5.4×10^{12} particles/m^3) was prepared, and the intensity ratio measured in that solution was converted to temperature using the calibration of Fig. 7, which was obtained for a 9 μg/mL solution (1.8×10^{12} particles/m^3). The optical path through the particle/water solution was 10 mm. A difference of only 1.2 K was observed, which indicate a negligible effect of the particles on the optical path under these conditions.

3.8. Measurements in optically accessible furnace in 300-900 K range

To study the performance of the phosphor for temperature measurements above 350 K, emission spectra were recorded from a bulk powder sample placed in the optically accessible furnace under pulsed excitation at a fluence of 1 mJ/cm^2. Normalised spectra at recorded at 100 K intervals are shown on Fig. 9. As shown the shift and broadening is continuous over the 300-900 K temperature range. It is also interesting to observe the presence of the 400 nm emission at room temperature which disappears at higher temperatures. Note that it is preferable for measurements at low temperatures to choose a filter for the shorter wavelength range which does not include the 400 nm emission. Were this so, the temperature sensitivity would slightly decrease in the 300 to 400 K range, since the signal increase due to the blue shift into this filter band would be partially offset by the disappearance of the 400 nm emission band. The transmission spectra for the filter combination used for the ratio imaging in section 3.5 are superimposed into the emission spectra of Fig. 9. The ratio of intensities for this combination obtained from spectral integration is shown in Fig. 10. The ratio changes by a factor 26 between room temperature and 900 K. Here a power law was used to fit the data, and the relative temperature sensitivity was derived by inversion of the power law, as in section 3.5. The temperature sensitivity decreases with temperature. From Fig. 9, we can anticipate that this drop of sensitivity would be less pronounced if the filter for the shorter wavelength range would extend to 400 nm as to take full advantage of the blue-shift. This would be at the cost of a slight sensitivity loss near room temperature since part of the 400 nm emission band would be included. The choice of filter should be carefully optimised over the temperature range of interest using a random uncertainty model which takes into account both
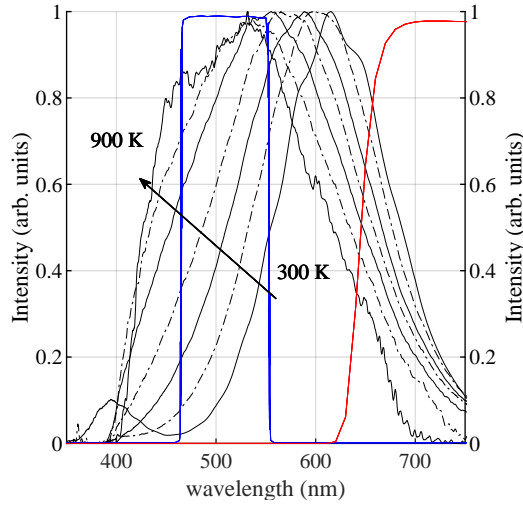
Fig. 9: Normalised luminescence emission spectra recorded from 300 to 900 K in furnace. The filters used in section 3.5 are also shown
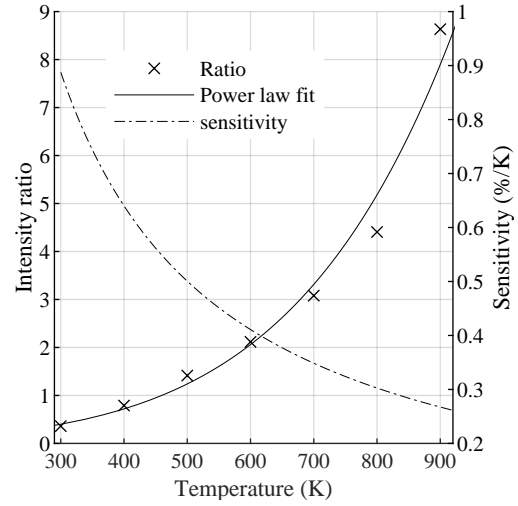
Fig. 10: Intensity ratio derived from the emission spectra and filter transmission curves of Fig. 9

temperature sensitivity and collection efficiencies as discussed in Ref. [1] (section 3.2.4).

The emission intensity measured by spectral integration of the whole emission band at each temperature is plotted on Fig. 11. As shown, there is an initial increase in emission intensity followed by a decrease from 500 K, which agrees with the observation made in Ref. [16] for the same dopant concentration. The T_{50} temperature can be estimated as approximately 650 K, and at 900 K the emission intensity is 4% of the room temperature value. For comparison, the thermal quenching curve of ZnO and BAM:Eu^{2+} are also plotted. SMP:Sn^{2+} and BAM:Eu^{2+} have very similar characteristics in this respect. The evolution of the lifetime with temperature is plotted in Fig. 12. As expected from the quenching curve (Fig. 11), the lifetime shortens significantly above 700 K and can be used for thermometry in this temperature range.

4. Discussion

Table 2 summarises the properties of the phosphor investigated here SMP:Sn^{2+} to those of the two previously characterised phosphors BAM:Eu^{2+} and ZnO in order to guide the choice of phosphors in specific thermometry applications. To anticipate the cost of using this phosphor in large experiments, it is important to note that the price per kg of powder is less than 100 euros.

Unlike the two previous phosphors which could be excited at both 355 nm and 266 nm, SMP:Sn^{2+} particles can only be efficiently excited at 266 nm. At low repetition rates, e.g. 10 Hz, delivering pulse energies of several mJ at 266 nm is straightforward. At kHz-rates, however, 266 nm excitation can be more complex than 355 nm excitation due to the increased absorption and therefore thermal loading of the laser components.

For phosphor particles to be used in turbulent flows, a high emission intensity and a short lifetime are necessary. In terms of brightness, a single SMP:Sn^{2+} particle emits a similar amount of photons as the two other phosphors. SMP:Sn^{2+} has a longer lifetime of 26 μs, which implies that for 85 % of the total intensity to be collected, a 50 μs exposure time is necessary. When using the particles as a tracer in a flow with a velocity of 10 m/s, a displacement of 500 μm would occur during this time, which imposes a limit on the signal or spatial resolution in fast flows. However,
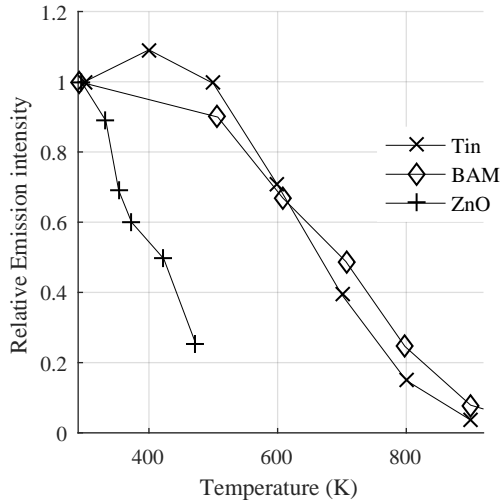
Fig. 11: Spectrally integrated luminescence emission intensity as a function of temperature for $(Sr,Mg)_3(PO_4)_2:Sn^{2+}$, for BAM:$Eu^{2+}$ in powder form [22], and from dispersed ZnO particles [9]
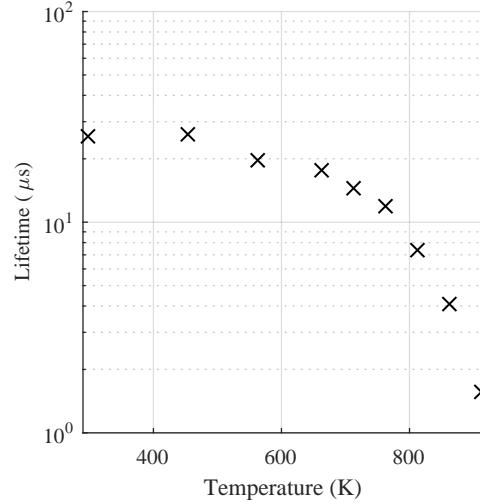

Fig. 12: Emission decay time (1/e) of SMP:Sn^{2+} over the 300-900 K range

in flows of moderate velocities, the lifetime and emission intensity of SMP:Sn^{2+} are suitable for fluid temperature measurements. In cases where short-lived fluorescence signals from windows or fuel species are present, the relatively longer lifetime can actually be advantageous when used in combination with a time-gating strategy. By delaying the exposure of the camera by a microsecond relative to the laser pulse, short-lived fluorescence signals can be avoided, while the useful signal from the phosphor is reduced by less than 3%. Details about this scheme will be presented in [28].

SMP:Sn^{2+} has a broad emission band centered at 614 nm, which allows a more efficient detection with non-intensified cameras compared to that of ZnO in the near-UV. The combination of red emission and long lifetime would in principle mean that the phosphor may be more prone to interferences from thermal radiation from hot surfaces, but considering the temperature range of those phosphors, this is unlikely to be an issue. At 900 K in a furnace, no interference could be detected.

In terms of thermometric performance, the temperature sensitivity measured in an imaging configuration with SMP:Sn^{2+} is 0.6%/K, which is 2.5 times higher than that of BAM:Eu^{2+} and only 15% lower than that of ZnO. However the collection efficiency of the chosen filters should also be compared, which was similar for the filter combination used in ZnO and SMP:Sn^{2+} experiments but substantially higher for BAM:Eu^{2+}. To more fairly compare the performance of the three phosphors, a random uncertainty model [22] taking into account the emission intensity per particle, the collection efficiency of the filters and the temperature sensitivity was employed. It was considered that a dichroic mirror would be used, as in [29], for all three phosphors to avoid the 50% loss. An otherwise identical measurement configuration (in terms of lens collection efficiency, seeding density, resolution and camera) was considered, which produces precision levels similar to those measured for BAM:Eu^{2+} in Ref [22]. The resulting numbers shown in Table 2 serve as a comparison between phosphors. SMP:Sn^{2+} affords a similar level of precision (4 K at 300 K) to ZnO.

Table 2: Summary of the luminescence properties of the three phosphor characterised in the fluid phase:

Phosphor	SMP:Sn^{2+}	BAM:Eu^{2+}	ZnO
Composition	$(Sr,Mg)_3$ $(PO_4)_2$:$Sn_{0.04}^{2+}$	$Ba_{0.88}MgAl_{10}O_{17}$:$Eu_{0.12}^{2+}$	ZnO (>99% pure)
Volume-equivalent diameter (μm)	2	2.4	1.2
Photoluminescence properties (at 300 K)			
Possible Nd:YAG excitation wavelengths (nm)	266	266 and 355	266 and 355
Photons per particle per pulse (at 20 mJ/cm^2 and 266 nm) [8]	2.3×10^6	2.7×10^6	3 ×10^6
Emission central wavelength (nm)	614	387	450
Full width at half maximum (nm)	124	15	50
1/e lifetime	26 μs	1 μs	<1 ns
Temperature sensitivity			
Temperature sensitivity measured in imaging configuration (over 20-60°C range, %/K)	0.6	0.24 [22]	0.7 [21]
Collection efficiency of filters used at 300	5% and 16 % (50% beamsplitter)	30% and 21% (dichroic beamsplitter) [22]	5% and 15% (50% beamsplitter) [21]
Predicted random uncertainty at 300 K in arbitrary configuration (K)	4.0	7.3	3.0
Quenching Temperature (T$_{50}$, K)	650	700 [1]	400 [21]
Cross-dependencies			
Fluence (at 20 mJ/cm^2)	0.6 K/10%	2 K/10%	6 K/10%
Particles on optical path	No evidence	No evidence	No evidence
Oxygen partial pressure	Not investigated	No (0-200 mbar)	Not investigated

However, above 475 K, the emission intensity of ZnO has decreased by 75% compared to the room temperature value, while for SMP:Sn^{2+} such decrease does not occur before 750 K. Above 475 K, it is interesting to compare the performance with that of BAM:Eu^{2+}, which presents similar quenching characteristics. At 700 K, the sensitivity of SMP:Sn^{2+} is still high 0.36%/K (Fig. 10) relative to that of BAM:Eu^{2+} which has dropped to 0.05 %/K [22]. By taking into account both thermal quenching and sensitivity, a 4-fold improvement in precision is expected with SMP:Sn^{2+} compared to BAM:Eu^{2+} at 700 K. It is therefore clear that SMP:Sn^{2+} offers the best sensing performance of all three phosphors over a wide temperature range.

Finally, the measurement uncertainty is not only related to signal statistics but can also be raised

by cross-dependencies of the measured quantity on other parameters, or by interferences from other light sources. As for the other phosphors investigated, no evidence were found of an effect of the number density of particles on the optical path on the measured temperature [21, 22, 24, 30]. Of particular importance is the sensitivity to the laser fluence, a parameter which can vary spatially and/or temporally in experiments. ZnO shows high sensitivity to laser fluence fluctuations, which means careful corrections are necessary in situations where there is a steady distribution in fluence. In applications where the laser fluence locally fluctuates, for example in liquid convection experiments, where strong index of refraction gradients are induced by density differences, the resulting error dominates and cannot be corrected for. In this respect, using SMP:Sn^{2+} particles, which exhibit a fluence sensitivity which is 10 times lower than that of ZnO, reduces this error contribution to a negligible level in comparison with the precision.

.

5. Conclusion

The phosphor $(Sr,Mg)_3(PO_4)_2$:Sn^{2+} was characterised for fluid thermometry and its thermometric performance compared to that of the two previously characterised phosphors $BaMgAl_{10}O_{17}$:Eu^{2+} and ZnO. The three phosphors all exhibit very different luminescence mechanisms resulting in varied luminescence properties. In cases where the flow is not too fast (<10 m/s) and excitation at 266 nm can be used, SMP:Sn^{2+} offers a temperature precision as good as that of ZnO at temperatures of 300-400 K, and almost 2 times better than BAM:Eu^{2+}. Over a larger temperature range up to 900 K, due a combination of favourable thermal quenching characteristics and high temperature sensitivity, SMP:Sn^{2+} offers a very substantial progress in terms of measurement precision, with a 4-fold decrease in random error relative to BAM:Eu^{2+}. In addition, the negligible dependence of SMP:Sn^{2+} on the laser fluence is essential in situations with large and uncontrollable excitation fluence fluctuations and is at minimum a significant advantage in most other measurement configurations, where controlling the laser fluence or correcting the measurements leads to lower signal levels or increased systematic error. The characterisation of this phosphor has improved and broadened the measurement capabilities of fluid thermometry using thermographic phosphors.

Acknowledgements

References

1. C. Abram, B. Fond, and F. Beyrau, "Temperature measurement techniques for gas and liquid flows using thermographic phosphor tracer particles," Prog. Energy Combust. Sci. **64**, 93 – 156 (2018).
2. A. O. Ojo, B. Fond, B. G. M. V. Wachem, A. L. Heyes, and F. Beyrau, "Thermographic laser doppler velocimetry," Opt. Lett. **40**, 4759–4762 (2015).
3. B. Fond, C. Abram, A. Heyes, A. Kempf, and F. Beyrau, "Simultaneous temperature, mixture fraction and velocity imaging in turbulent flows using thermographic phosphor tracer particles," Opt. Express **20**, 22118–22133 (2012).
4. W. A. Miller and M. Keyhani, "The correlation of simultaneous heat and mass transfer experimental data for aqueous lithium bromide vectical falling film absorption," J. Sol. Energy Eng. **123**, 30–42 (2001).
5. N. Neal, J. Jordan, and D. Rothamer, "Simultaneous measurements of in-cylinder temperature and velocity distribution in a small-bore diesel engine using thermographic phosphors," SAE Int. J. Engines **6**, 19pp (2013).
6. P. Schreivogel, C. Abram, B. Fond, M. Straußwald, F. Beyrau, and M. Pfitzner, "Simultaneous khz-rate temperature and velocity field measurements in the flow emanating from angled and trenched film cooling holes," Int. J. Heat Mass Transf. pp. 390–400 (2016).
7. J. Brübach, C. Pflitsch, A. Dreizler, and B. Atakan, "On surface temperature measurements with thermographic phosphors: A review," Prog. Energ. Combust. **39**, 37–60 (2013).

8. B. Fond, C. Abram, M. Pougin, and F. Beyrau, "Characterisation of dispersed phosphor particles for quantitative luminescence measurements," Opt. Mater. (in revisions) .

9. C. Abram, B. Fond, and F. Beyrau, "High-precision flow temperature imaging using ZnO thermographic phosphor tracer particles," Opt. Express **23**, 19453–19468 (2015).

10. G. Blasse and B. Grabmaier, *Luminescent Materials* (Springer, 1994), 2nd ed.

11. H. Koelmans and A. P. M. Cox, "Luminescence of modified tin activated strontium orthophosphate," J. The Electrochem. Soc. **104**, 442–445 (1957).

12. J. F. Sarver, M. V. Hoffman, and F. A. Hummel, "Phase equilibria and tin activated luminescence in strontium orthophosphate systems," J. Electrochem. Soc. **108**, 1103–1110 (1961).

13. A. Bril and W. Hoekstra, "Efficiencies of phosphors for short-wave ultra-violet excitation," Philips Res. Repts **16**, 356–370 (1961).

14. S. Parke and R. S. Webb, "Optical properties of sn 2+ and sb 3+ in calcium metaphosphate glass," J. Phys. D: Appl. Phys. **4**, 825 (1971).

15. M. Leskelǎ, T. Koskentalo, and G. Blasse, "Luminescence properties of Eu^{2+}, Sn^{2+}, and Pb^{2+} in SrB_6O_{10} and $Sr_{1-x}Mn_xB_6O_{10}$," J. Solid State Chem. **59**, 272 – 279 (1985).

16. W. Yen, S. Shionoya, and H. Yamamoto, *Phosphor Handbook* (CRC Press, 2007), 2nd ed.

17. G. Bizarri and B. Moine, "On phosphor degradation mechanism: thermal treatment effects," J. Lumin. **113**, 199 – 213 (2005).

18. A. Yánez-González, B. van Wachem, S. Skinner, F. Beyrau, and A. Heyes, "On the kinetics of thermal oxidation of the thermographic phosphor $BaMgAl_{10}O_{17}$:Eu," Mater. Des. **108**, 145 – 150 (2016).

19. Z. Yin, B. Fond, G. Eckel, C. Abram, W. Meier, I. Boxx, and F. Beyrau, "Investigation of $BAM:Eu^{2+}$ particles as a tracer for temperature imaging in flames," Combust. Flame **184**, 249 – 251 (2017).

20. B. Fond, C. Abram, and F. Beyrau, "On the characterisation of tracer particles for thermographic particle image velocimetry," Appl. Phys. B-Lasers O **118**, 393–399 (2015).

21. C. Abram, M. Pougin, and F. Beyrau, "Temperature field measurements in liquids using zno thermographic phosphor tracer particles," Exp. Fluids **57**, 1–14 (2016).

22. B. Fond, C. Abram, and F. Beyrau, "Characterisation of the luminescence properties of $BAM:Eu^{2+}$ particles as a tracer for thermographic particle image velocimetry," Appl. Phys. B-Lasers O **121**, 495–509 (2015).

23. F. T. Rabouw, P. T. Prins, P. Villanueva-Delgado, M. Castelijns, R. G. Geitenbeek, and A. Meijerink, "Quenching pathways in nayf4:er3+,yb3+ upconversion nanocrystals," ACS Nano **12**, 4812–4823 (2018).

24. D. Witkowski and D. A. Rothamer, "Investigation of aerosol phosphor thermometry (apt) measurement biases for eu:bam," Appl. Phys. B **124**, 202 (2018).

25. J. Grafmeyer, J. Bourcet, J. Janin, J. Denis, and J. Loriers, "Luminescence properties of Sb^{3+} in yttrium phosphates," J. Lumin. **11**, 369 – 380 (1976).

26. D. W. Cooke, B. L. Bennett, K. J. McClellan, J. M. Roper, and M. T. Whittaker, "Oscillator strengths, Huang-Rhys parameters, and vibrational quantum energies of cerium-doped gadolinium oxyorthosilicate," J. Appl. Phys. **87**, 7793–7797 (2000).

27. H. Donker, W. M. A. Smit, and G. Blasse, "On the luminescence of some tin-activated alkaline-earth orthophosphates," J. Electrochem. Soc. **136**, 3130–3135 (1989).

28. A. Mendieta, B. Fond, P. Dragomirov, and F. Beyrau, "A time-gated approach for improved ratio-based phosphor thermometry of fast heat transfer phenomena," submitted to Meas. Sci. Technol. .

29. C. Abram, B. Fond, A. Heyes, and F. Beyrau, "High-speed planar thermometry and velocimetry using thermographic phosphor particles," Appl. Phys. B-Lasers O **111**, 155–160 (2013).

30. E. Hertle, S. Will, and L. Zigan, "Characterization of yag:dy,er for thermographic particle image velocimetry in a calibration cell," Meas. Sci. Technol. **28**, 025013 (2017).